Optical Frequency Domain Reflectometer Distributed Sensing Using Microstructured Pure Silica Optical Fibers Under Radiations

S. Rizzolo, A. Boukenter, T. Allanche, J. Périsse, G. Bouwmans, H. El Hamzaoui, L. Bigot, Y. Ouerdane, M. Cannas, M. Bouazaoui, et al.

Optical Frequency Domain Reflectometer Distributed Sensing Using Microstructured Pure Silica Optical Fibers under Radiations

S. Rizzolo, *Student Member, IEEE*, A. Boukenter, T. Allanche, J. Périsse, G. Bouwmans, H. El Hamzaoui, L. Bigot, Y. Ouerdane, M. Cannas, M. Bouazaoui, J-R Macé, S. Bauer and S. Girard, *Senior Member, IEEE*

Abstract- **We investigated the capability of micro-structured optical fibers to develop multi-functional, remotely-controlled, Optical Frequency Domain Reflectometry (OFDR) distributed fiber based sensors to monitor temperature in nuclear power plants or high energy physics facilities. As pure-silica-core fibers are amongst the most radiation resistant waveguides, we characterized the response of two fibers with the same microstructure, one possessing a core elaborated with F300 Heraeus rod representing the state-of-the art for such fiber technology and one innovative sample based on pure sol-gel silica. Our measurements reveal that the X–ray radiations do not affect the capacity of the OFDR sensing using these fibers to monitor the temperature up to 1 MGy dose whereas the sensing distance remains affected by RIA phenomena.**

***Index Terms*—Optical fiber sensors, radiation, Rayleigh scattering.**

I. Introduction

During the last decades the interest on fiber-based devices increased their demand for several applications such as sensors, diagnostics…, in particular for their employment in harsh environments associated with nuclear power plants, space or high energy physics facilities [1]. Thanks to some fibers advantages such as fast response, reduced volume and weight, several techniques are developed for monitoring different environmental parameters such as temperature, strain and radiation dose by replacing punctual sensor technologies by one sensor exploiting the whole optical fiber length sensitivity to external change [2] in a discrete way as the case of Fiber Bragg Gratings (FBGs) [3] or with distributed measurements based on scattering mechanisms [4]-[8].

In the panorama of fiber-based distributed sensing techniques several studies are devoted to investigate the employment of these sensors classes in harsh environments [4]-[8]. In particular, X. Phéron *et al.* [4] reported that Brillouin based sensors are affected by radiation because it induces an additional Brillouin frequency shift (BFS) that affects temperature and strain measurements. On the other hand, Radiation Induced Attenuation (RIA) degrades the response of Raman temperature based sensors by degrading differently the Stokes and Anti-Stokes signals [5], [6]. OFDR is one of the most promising techniques since it offers the best spatial resolution of few µm over 70 m of fiber length [9]. Moreover, our recent study showed that radiation does not affect Rayleigh mechanisms at the basis of this technique: indeed, temperature and strain coefficients remain unchanged, within the 5%, of error up to 10 MGy (SiO_2) for a large variety of standard fiber classes [7]. However, the potentialities of OFDR sensors are affected by RIA phenomena [7] which limits the sensing range. Therefore, before integration of the OFDR-based systems in harsh environments, their tolerance to the constraints associated with high levels of radiations have to be demonstrated.

The parameters having significant effects on RIA are well known, a very influential one concerns the nature of the dopants used to modulate the refractive index profile of the fiber core and cladding [10], [11]. Radiation also, can introduce structural changes in glass matrix by varying locally refractive index and modifying the scattering amplitude as a function of the length for a given fiber. In terms of optical fiber sensors (OFSs) performances, these changes can influence Rayleigh distributed measurements introducing errors in the measurement of controlled parameter, especially for *in situ* measurements.

The development of microstructured optical fibers (MOFs) is one of the most innovative progresses in the field of optical waveguides. These fibers present wavelength scale structures with a refractive index contrast that provides them unusual properties [12]. Two types of MOFs are usually distinguished: photonic bandgap (PBG) MOFs in which the light remains confined in a low index core thanks to a PBG cladding and high index core fibers in which the light is guided via modified total internal reflection (MTIR).

S. Rizzolo is with Univ-Lyon, Lab. Hubert Curien, CNRS UMR 5516, F-42000 Saint-Etienne, France, with Dipartimento di Fisica e Chimica, Università degli Studi di Palermo, 90100 Palermo, Italy and also with AREVA NP (e-mail: serena.rizzolo@univ-st-etienne.fr).

A. Boukenter, T. Allanche, Y. Ouerdane, S. Girard are with Univ-Lyon, Lab. Hubert Curien, CNRS UMR 5516, F-42000 Saint-Etienne, France.

G. Bouwmans, H. El Hamzaoui, L. Bigot, M. Bouazaoui are with PhLAM Laboratory, Université de Lille 1-Sciences et Technologies, CNRS UMR 8523, F-59650 Villeneuve d'Ascq, France

M. Cannas is with Dipartimento di Fisica e Chimica, Università degli Studi di Palermo, 90100 Palermo, Italy.

J. Perisse, J-R Macé and S. Bauer are with AREVA, France.

In literature, the transient radiation response of hollow core PBG (HC-PBG) fibers [13] is discussed and their steady state radiation responses have been presented by G. Cheymol et al. in [14]-[16]. From these studies, it appears that HC-PBG fibers are very promising for integration in steady state high dose level radiation environments where they exhibit RIA as low as 2.1 dB/km after 1 MGy at 1550 nm [16]. However the results are more complex for transient - or pulsed–irradiation, as discussed in [13]. Furthermore, several issues limit the use of HC-PBG fiber such as the reliability, the splicing with other fibers, sources or detectors and their high costs. On the other hand, MTIR MOFs are easier to handle and present several useful properties that could be exploited to design new laser or plasma fiber-based diagnostics. Depending on their micro-structuration, such fibers can be endlessly single-mode, present less sensitivity to bending loss, larger mode field diameters to limit non-linear phenomena occurring at high signal power. Another possible advantage, under irradiation and for fiber sensing, consists in their homogeneity in terms of glass properties. Such fibers can be made of a unique glass composition, without dopants or impurities to limit the fiber transmission degradation [10] or to limit the residual strain resulting from the different properties of core and cladding. To our knowledge, only a few studies have been devoted to the radiation response of this class of waveguides [17]-[19]. In [17], a prototype MOF was tested and its high radiation sensitivity was attributed to the silica glass tubes used to design the fiber, the tested fiber being no more representative of today's advances. More complete comparative studies between MOFs and conventional fibers showed that pure-silica or fluorine doped MOFs, which offers specific advantages compared to conventional fibers, are promising for use in harsh environments as the ones associated with Megajoule class lasers due to their radiation tolerance [18] [19].

In this work we study the steady state effects on Rayleigh radiation response of MOFs for distributed temperature and strain sensors up to 1 MGy dose levels. In particular, we explored the performances of Sol Gel originated MOFs, a promising technique that permits to obtain several classes of fibers with unique optical properties [20] [21]. Up to the best of our knowledge, this is the first study combining OFDR technique with MOFs, and for this reason we focused our attention on two pure silica core (PSC) samples that are known to be among the most radiation resistant classes of fibers, to compare our results with their standard counterpart. The goal of this work was to investigate on sensing capability of MOFs adapted for radiation applications. For this, we experimentally determined the temperature sensitivity coefficient of the two MOF samples before and after irradiation and we compared, during irradiation, the temperature changes monitored by thermocouple and through our OFDR sensor probing the added values of MOF fibers. A characterization of spectral RIA and its kinetic are also reported to evaluate the RIA related limitation that will lead to a comprehension on the work to be done for the integration of MOF distributed sensors in harsh environments.

II. Material and methods

A. Investigated samples

The two investigated air/silica MOFs have been fabricated by the PhLAM-IRCICA laboratory in Lille (France) by the stack and draw technique. Both fibers present the same microstructured geometry, reported in Fig. 1 (a), with a hole diameter of 1.8 µm and a pitch Λ =3.9µm. The two fibers are made of different pure silica classes.

MOF1 is entirely made of pure-silica glass F300 tubes (Heraeus) with an adapted procedure to ensure a limited concentration of OH group at the tube surfaces that causes an excess of optical losses. The optical losses in this fiber (MOF1) are around 4 dB/km at 1550 nm.

MOF2 fiber core originates from Sol-Gel silica at low OH(<1ppm) [22] concentration and is combined to F300 Hereaus silica capillaries for the cladding region. Since no special cleaning procedure was applied to the sol-gel silica rod, the attenuation of this fiber (MOF2) is around 20 dB/km at 1550 nm. Fig. 1 (b) and Fig. 1 (c) report a 2D mapping of PL intensity around 400 nm under 325nm laser excitation in the microstructured cladding from -30 µm to 30 µm in both x and y direction with a step of 1.5 µm. This study highlights the presence of some emitting centers in the non-irradiated MOFs at the border of microstructured region due to processes fabrication.

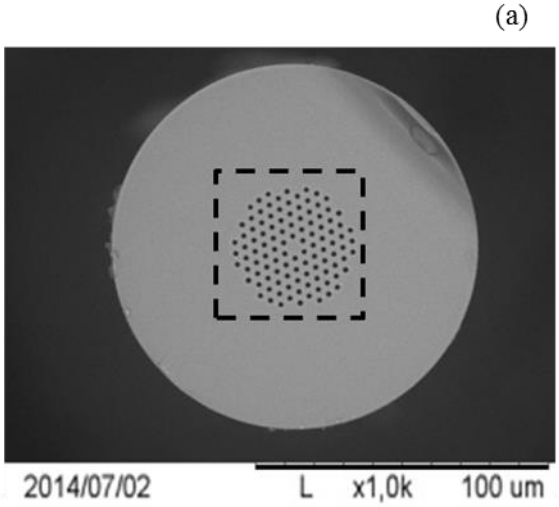

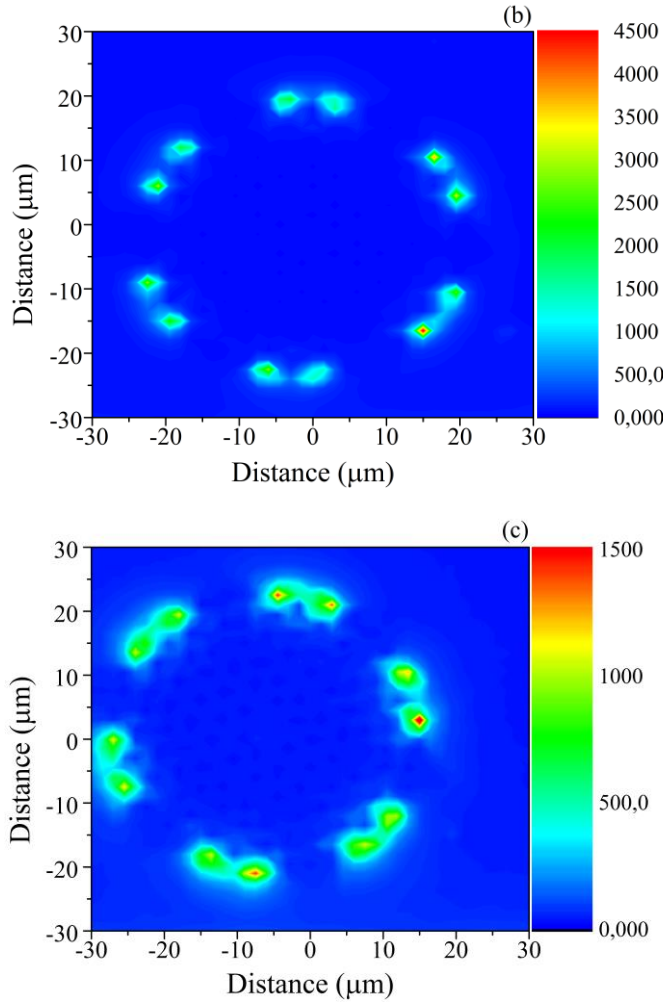

Fig. 1 SEM images of the MOF1 fiber that is representative of the structure of both tested samples (a); A mapping of luminescence around 400 nm under 325nm excitation of in the microstructured part of the samples (highlighted by dotted square in (a)) is reported in (b) and (c) for MOF1 and MOF2 respectively, to evidence the presence of some emitting sites at the border of microstructured region.

If we compare Fig. 1 (a) with Fig. 1 (b) and Fig. 1 (c) we can note that the presence of these centers is correlated with the presence of the most extern microstructured region: the centers appear in the region where the holes are not present. Likely, used tubes in the fabrication process presented some impurities inside that may cause the PL showed in Fig. 1 (b) and Fig. 1 (c). However, these emitting centers are far from the region of light propagation, thus not influencing the optical properties in the core.

B. *Irradiation facilities*

We investigate steady state as well as permanent radiation effect performing X-ray irradiations with the X-ray source facility (MOPERIX) in Laboratoire Hubert Curien (Saint Etienne, France). The dose-rate is evaluated with a probe in different points of the irradiation chamber, where cartography was performed. By a statistic done on obtained values in the chosen uniform region, we evaluate the dose-rate in our experiments that is (3.2±0.1) Gy(SiO_2)/s and the reached dose is 1 MGy(SiO_2). Irradiations were performed at room temperature controlled by a K type thermocouple to register the fluctuation over time from day to night inside irradiation chamber.

C. *Distributed temperature measurements*

Distributed sensing measurements were done with an Optical Backscatter Reflectometer (OBR) 4600 from Luna Technologies. In all measurements described below the laser source was tuned over a range of 21 nm with a center wavelength around 1550 nm (with accuracy of 1.5 pm), yielding to a nominal spatial resolution of the Rayleigh scatter pattern of 40 µm along the investigated optical fiber propagation axis.

In situ OBR measurements were performed under X-ray irradiation on ~1 m -long fiber spooled on an aluminum plate in a circular zone of constant dose rate with a diameter of 8 cm. The acquisition is made every 5 sec during the first period of irradiation and then each 5 minutes; temperature is monitored by the comparison with a type K thermocouple data stuck on the same plate inside irradiation zone and close to the fiber.

Temperature calibration was done in an oven controlled by a type K thermocouple after irradiation; an example of recorded spectral shift as a function of optical fiber length is reported in Fig. 2 for non-irradiated and irradiated part in the different temperature steps. For such experiments, the samples of the same fiber type, both non-irradiated and irradiated one, were tested together (the total length of the sample was ~2m) to perform the temperature treatment at the same time. C_T was deduced from the slope of the Rayleigh spectral shift with temperature in the range from 30 °C up to 70 °C with a ΔT of 5 °C.

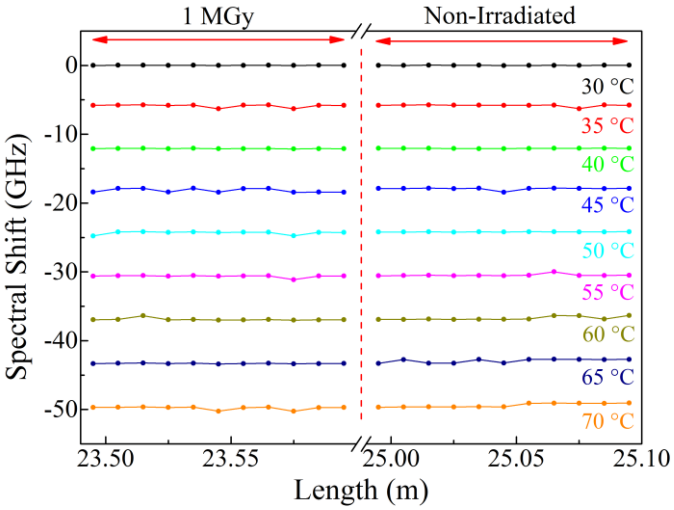

Fig. 2 Rayleigh spectral shift in the non-irradiated and 1 MGy irradiated MOF1 as a function of the path length at 9 different temperatures from 30 °C (reference trace) to 70 °C.

D. *Confocal micro-luminescence investigation*

The permanent irradiation effects were studied via confocal micro-photoluminescence (PL) by using a LabRam Aramis spectrometer, equipped with a He-Cd ion laser probe emitting at 3.82 eV (325 nm), a x40 objective and micro-translation stages. The corresponding spatial resolution was about 1.5 µm.

The CML measurements are performed for both samples, before and after irradiation, the same experimental conditions

(e.g. same length of the samples that were ~3 mm long, same days to assure not fluctuation of the laser source …), to compare the two samples as well as the non-irradiated irradiated fiber luminescence properties.

E. RIA measurements

In addition to the previously described tests, the same fibers were characterized with another setup allowing the measurement of the temporal (5 s time resolution) and spectral dependence (900-2200 nm) of the RIA during and after the X-ray exposure. To this end, we used a laser-driven light source (EQ99 from Energetiq) and a near-IR spectrophotometer NIRQuest 512. For these measurements the samples are 20 m long and the temperature is monitored during the measurements with a type K thermocouple.

III. Experimental Results

A. Evaluation of sensor performances

Temperature characterization on non-irradiated MOFs is shown in Fig. 3 where measured Rayleigh spectral shift as a function of temperature is reported together with linear fits for both samples. We observe a linear dependence in the two fibers, providing evidence for the potential of such fibers for temperature measurements. Extracted coefficients are obtained by making an average of the values obtained in each sensing point. We find close coefficients for the two fibers: (6.40±0.04) $°C^{-1}$ for MOF1 and (6.44±0.01) $°C^{-1}$ in MOF2, the errors being obtained from standard deviation on all the values. These values of C_T are used to calculate the temperature of MOFs sensors during irradiation.

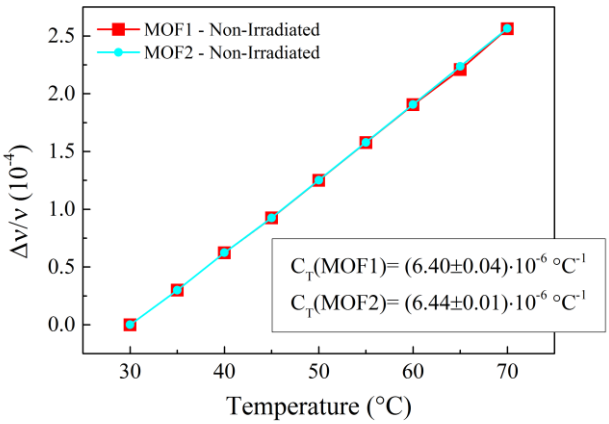

Fig. 3 Rayleigh spectral shift dependences on temperature for MOF1 (red circles) and MOF2 (blue circles) with respective linear fits (red and blue straight lines) before irradiation.

To investigate the steady state radiation effect on OFDR measurements, we irradiated our samples up to a total dose of ~1 MGy(SiO_2) at a dose rate of (3.2±0.1) Gy/s through 87 hours run duration. In Fig. 4 are reported the obtained results for MOF1. We followed at the same time the temperature evolution with a thermocouple placed near the fiber in the irradiation zone. The temperature profiles obtained with the fiber and the thermocouple are shown in Fig. 4 (a), where fiber temperature was obtained by an average along the fiber segment under irradiation. We find that profiles are close and we are able to follow temperature increase during the first minutes of irradiation (due to the switch on of the X-ray tube) as well as temperature fluctuation from day to night inside the chamber. By comparing the temperatures measured by OFDR and the thermocouple we calculate the ΔT to highlight the possible differences caused by the irradiation. Results are shown in Fig. 4 (b) evidencing that radiation does not affect Rayleigh temperature measurements: indeed, except for a small decrease during the first minutes of irradiation, ΔT remains constant around the value of (-0.27±0.06) °C during the whole irradiation time.

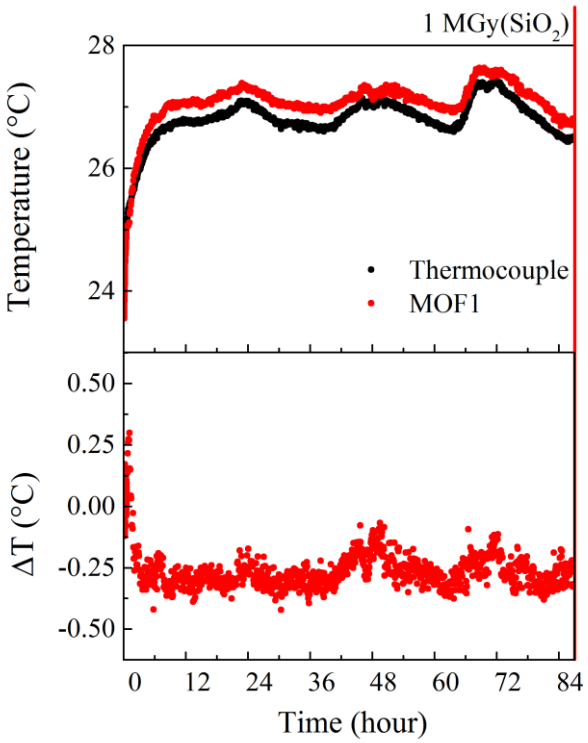

Fig. 4 (a) Temperature profiles obtained from MOF1 (red circles) and thermocouples (black circles) data and (b) differences between OFDR and thermocouple measurements as a function of time during irradiation (up to 1 MGy(SiO_2) dose).

We found that temperature measured by OBR well agree with thermocouple one; however some differences are present between the two profiles. To better understand on the origin of this variation we show in Fig. 5 the temperature as a function of fiber length in MOF1 before the irradiation and for several doses up to 1 MGy. We can see that temperature is not homogeneous along the sample, with fluctuation from 0.7 °C at 10 kGy to 2 °C at 1 MGy. This profile can due to variation in the temperature in the irradiation chamber, since that temperature at the fiber level was not imposed by external devices, but also to the presence of some stressed parts in the spool that evolve with the time. Indeed, we note that temperature distribution remains more or less the same with the increasing of the doses.

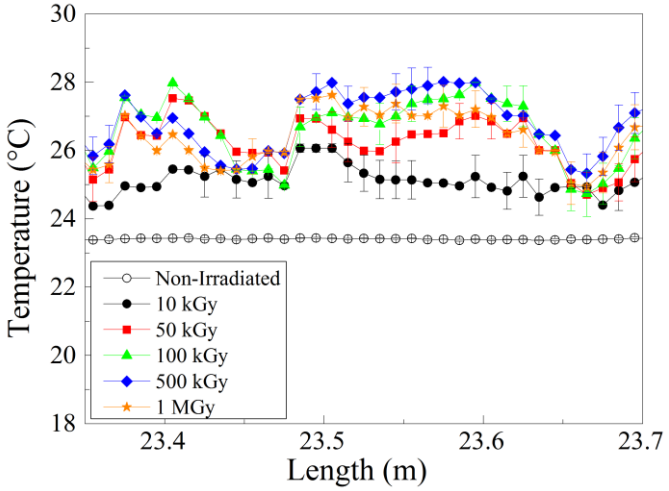

Fig. 5 Temperature distribution along the fiber length in MOF1 for non-irradiated sample (open black points) and sample irradiated at 10 kGy (black points), 50 kGy (red points), 100 kGy (green points), 500 kGy (blue points) and 1 MGy (orange points).

The same investigation was carried out for MOF2 and the results are reported in Fig. 6 and Fig. 7.

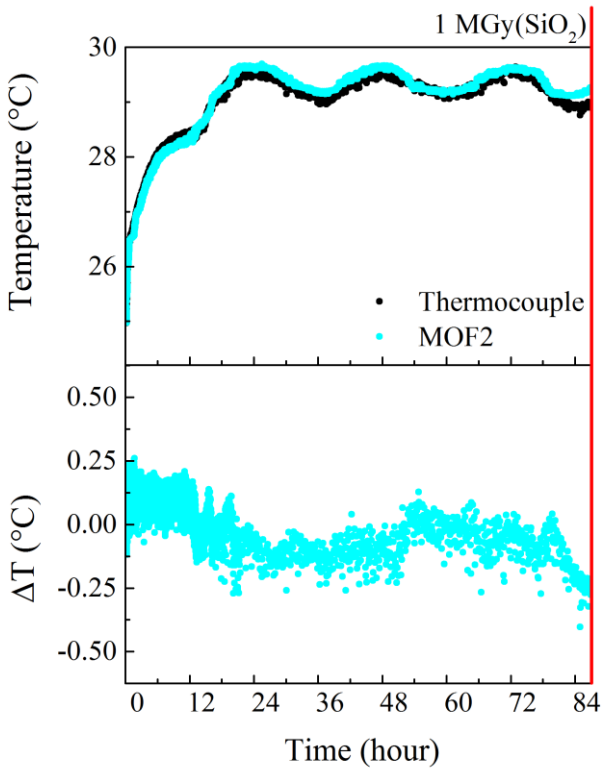

Fig. 6 (a) Temperature profiles obtained from MOF2 (blue circles) and thermocouples (black circles) data and (b) differences between OFDR and thermocouple measurements as a function of time during irradiation (up to 1 MGy(SiO_2) dose).

As before, we see that OFDR and thermocouple temperature profiles match each other [Fig. 6 (a)] during the entire irradiation time, giving the possibility to detect temperature variation due to turning on of radiation as well as from day to night temperature changes. ΔT values in Fig. 6 (b) show that no radiation effects influence temperature measurements for MOF2 being variations scattered around 0 °C (with higher dispersion of 0.2 °C).

Temperature distribution along the fiber length is reported in Fig. 7 for non-irradiated MOF2 and sample irradiated at different doses. Here, we can see better what we already observe in MOF1. Indeed, temperature profiles along the fiber are the sample at the different doses. We can also note that between (13.40±0.01) m and (13.58±0.01) m the fiber temperature is substantially different from the other part of the sample. It is possible that when we stuck the fiber on the aluminum plate we apply some stress that evolves with time, thus leading to recorded variation. If we do not take in account this part of the sample, we obtain temperature variation along the fiber profile of 0.7 °C for all the doses.

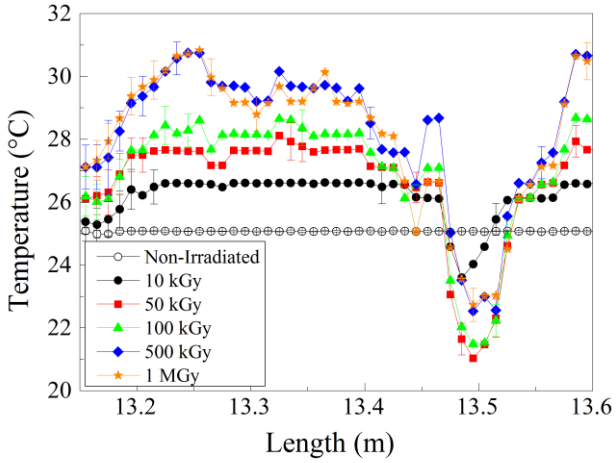

Fig. 7 Temperature distribution along the fiber length in MOF2 for non-irradiated sample (open black points) and sample irradiated at 10 kGy (black points), 50 kGy (red points), 100 kGy (green points), 500 kGy (blue points) and 1 MGy (orange points).

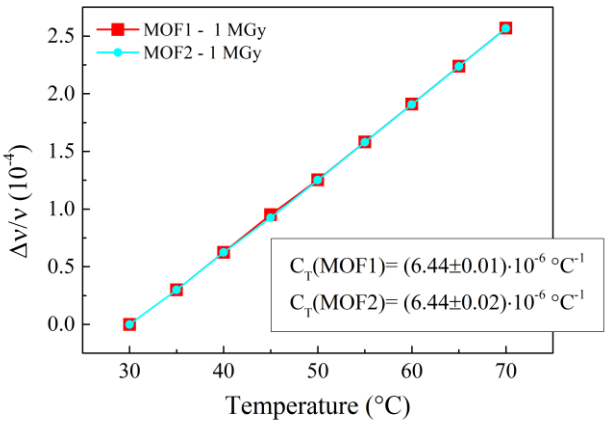

Fig. 8 Rayleigh spectral shift dependences on temperature for MOF1 (red circles) and MOF2 (blue circles) with respective linear fits (red and blue straight lines) after irradiation.

After irradiation we performed a new temperature calibration to evaluate possible changes in C_T. Linear fits on Rayleigh spectral shift dependence on strain illustrated in Fig. 6. give C_T values of (6.44±0.01) $°C^{-1}$ in MOF1 and

(6.44±0.02) °C^{-1} in MOF2 highlighting that radiation does not induce changes in temperature calibration curves.

B. Investigation on radiation induced MOF changes

Spatial distribution of radiation induced defects was studied over the transverse fiber section, thanks to the confocal micro-luminescence setup. Fig. 9 (a) shows typical PL spectra emitted from the core center and microstructured part of the cladding, in a region without holes, for non-irradiated and irradiated MOF1 at 1 MGy(SiO_2). Spectra exhibit a band peaked at 650 nm related to non-bridging hole oxygen centers (NBOHC) [24, 25] that is around 3 times more intense in the core center than in the cladding for irradiated sample whereas no PL luminescence in highlighted from non-irradiated one. The map of the PL intensity around 650 nm is reported in Fig. 9 (b), in the microstructured cladding and core of MOF1, showing that NBOHCs are concentrated in the core region even if a smaller amount of defects was induced by radiation also in the cladding.

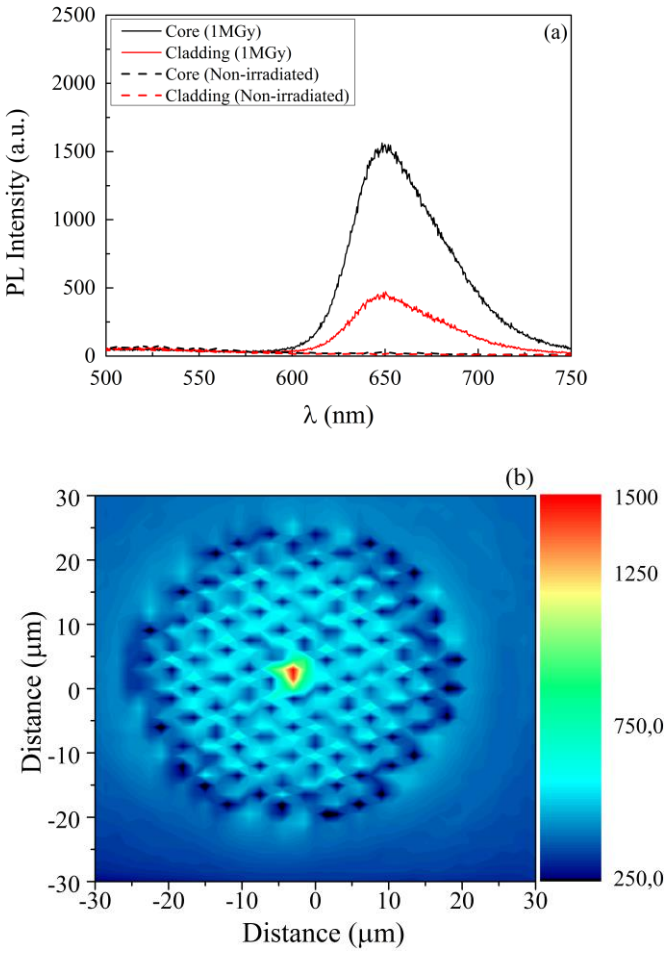

Fig. 9 (a) PL spectrum emitted from 1 MGy(SiO_2) MOF1 (solid line) and non-irradiated (dotted line) from the core center (black) and the cladding (red) under excitation at 325 nm. (b) Map of the PL intensity around 650 nm in the 1 MGy(SiO_2) MOF1 shows that concentration of emitting centers around 650 nm is higher in the fiber core.

PL spectra emitted from the core center and microstructured part of the cladding in non-irradiated and irradiated at 1 MGy(SiO_2) samples, as well as the map of PL intensity around 650 nm for irradiated MOF2 are reported respectively in Fig. 10 (a) and Fig. 10 (b). Here again, we find the NBOHCs that are distributed in the microstuctured region with a maximum concentration in the solid pure silica core.

The maps of the PL intensity around 400 nm in the samples irradiated at 1 MGy(SiO_2) are not changed from those reported in pristine samples in Fig. 1 (a) and Fig. 1 (b) showing the presence of some blue emitting centers at the border of microstructured region due to stack and drawn fabrication processes that remain unaffected by radiations.

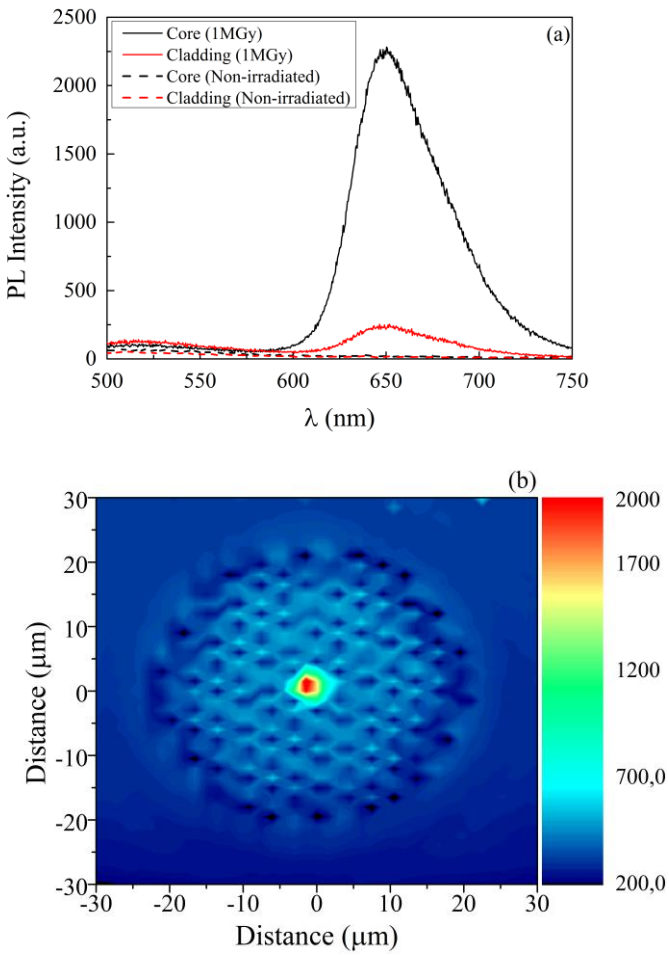

Fig. 10 (a) PL spectrum emitted from 1 MGy(SiO_2) MOF1 (solid line) and non-irradiated (dotted line) from the core center (black) and the cladding (red) under excitation at 325 nm. (b) Map of the PL intensity around 650 nm in the 1 MGy(SiO_2) MOF1 shows that concentration of emitting centers around 650 nm is higher in the fiber core.

IV. Discussion

Confocal micro luminescence investigation revealed that X-rays induce point defects in our MOFs: NBOHCs are created during irradiation with distribution of these defects [as shown in Fig. 9 (b) and Fig. 10 (b)] being more concentrated in the core, phenomenon that can be due to a collapse of the core occurred during the fabrication of MOFs.

It is known that radiation affects the OFDR-sensor response: a factor which limits their employment in presence of radiation is RIA by reducing the sensing range [7]. For our 70 m sensing range, considering that the maximum total losses permitted by the OFDR are 10 dB, we investigate the RIA in the infrared part of the spectrum to estimate the integration of such sensors in radiation environments. The results highlight that high level of online RIA are reached at 1 MGy(SiO2) for both fibers. Fig. 11 reports online spectral RIA measurements at different accumulated doses from 1.2 µm up to 2 µm, compared with the maximum values of RIA (highlighted with grey straight line) permitting to use OFDR-based sensors for MOF1.

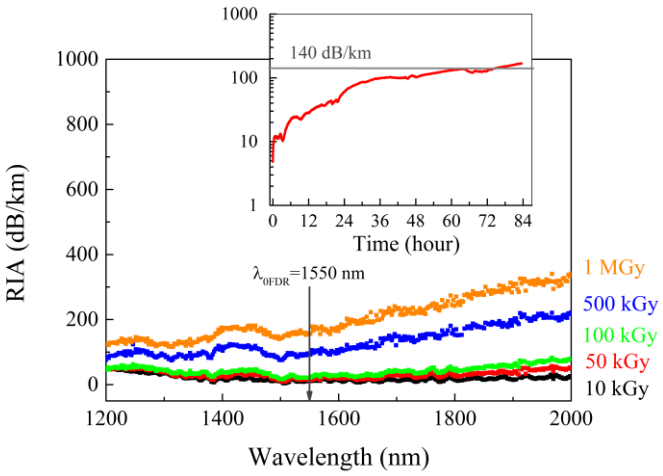

Fig. 11 Online radiation induced attenuation spectra in the infrared region for MOF1 at different reached total doses from 10 kGy(SiO_2) which is the lowest curve (black squares) up to 1 MGy(SiO_2) that corresponds to the highest one (orange squares). The inset shows RIA as a function of time during irradiation up to 1 MGy(SiO_2) where the losses reach the value of ~150 dB/km; the gray straight line at 140 dB/km highlights the maximum OFDR permitted optical losses at the operating wavelength (1550 nm) for 70 m of sensing length.

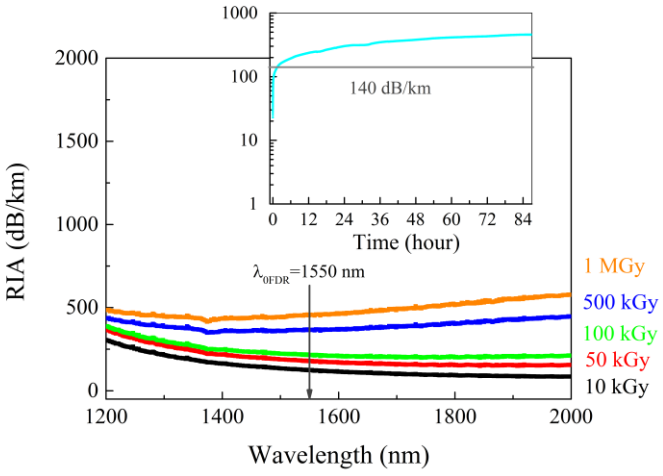

Fig. 12 Online radiation induced attenuation spectra in the infrared region for MOF2 at different reached total doses from 10 kGy(SiO_2) which is the lowest curve (black squares) up to 1 MGy(SiO_2) that corresponds to the highest one (orange squares). The inset shows RIA as a function of time during irradiation up to 1 MGy(SiO_2) where the losses reach the value of ~400 dB/km; the gray straight line at 140 dB/km highlights the maximum OFDR permitted optical losses at the operating wavelength (1550 nm) for 70 m of sensing length.

We see that RIA increases with the wavelength, excluding that the tails of UV-Visible absorption defects-related bands can act as the main contributor to this attenuation. We note that all the curves, except the one corresponding to 1 MGy(SiO2), are below 140 dB/km. Looking better into the kinetics indeed, we see that, at 1550 nm (inset of Fig. 11), radiation induced losses increase with the irradiation time up to reach a value of ~ 150 dB/km at 1 MGy(SiO2), thus limiting the sensing length to ~ 65 m. In the case of MOF2 (see Fig. 12), we obtain RIA values of ~ 400 dB/km that drastically decrease the sensing range of the sensor to 25 m thus limiting the employment of such fiber types when higher tolerance is requested. We note that RIA results agree with CML ones, shown in Fig. 9 and Fig. 10, highlighting that Sol-Gel fiber (MOF2) is more sensitive to radiation than the F300-based one.

V. Conclusion

In conclusion, obtained results show that OFDR-based sensors exploiting MOF fibers are not affected by radiation-induced errors as it is the case of FBGs, Brillouin, Raman sensors. It is known in literature that for FBGs with the radiation induces a Bragg Wavelength Shift (BWS) that depends on fiber composition [3], Brillouin sensors are affected by radiation with the Radiation Induced Brillouin Frequency Shifts (RI-BFS) [4] and Raman sensors by the $\Delta\alpha$ affecting the ratio between Stokes and Anti-Stokes wavelengths [5], [6]. For OFDR measurements instead we find that temperature profiles are well determined in both samples with variation from thermocouple reference data giving an error on distributed temperature measurement of ~0.3 °C. More, temperature calibration curves show that C_T value remains unchanged (within the experimental error) after the irradiation up to 1 MGy(SiO_2), results that are consistent with the previous one reported in [23] where the same samples were irradiated up to 50 kGy during a 3 hours long run. We see indeed that, distributed sensing is possible within an error the same incertitude when the temperature inside the irradiation chamber is not stable as well for longer irradiation period, permitting to appreciate the from day to night temperature variation.

The results highlighted by RIA measurements show, however, that employment of MOFs is limited by the attenuation. In particular, Sol-Gel microstructured optical fibers are more sensitive to radiation than their standard counterpart.

It is worth to mention that, an improvement in terms of optical losses and sensitivity to radiation, by applying an appropriate cleaning procedure to the sol-gel silica rod that constitute the fiber core, has to be achieved to extend the employment of MOFs to the majority of radiation applications but, even with reported performances, the development of OFDR sensing based on microstructured pure silica optical fibers in harsh environment that seems very promising up to the studied doses for fiber length of ~20 m.

VI. Acknowledgments

The authors from PhLAM laboratory would like to thank K. Delplace for technical assistance. The authors acknowledge the financial support of the French national research agency through the NANOFIBER project (ANR-12-RMNP-0019). This work was supported by French National Research Agency through Labex CEMPI (ANR-11-LABX-0007) and Equipex FLUX (ANR-11-EQPX-0017), through Contrat de Projets Etat Région (CPER) "Photonics for Society"

References

[1] Francis Berghmans, Benoît Brichard, Alberto Fernandez Fernandez, Andrei Gusarov, Marco Van Uffelen, Sylvain Girard , "An Introduction to Radiation Effects on Optical Components and Fiber Optic Sensors," in Optical Waveguide Sensing and Imaging, Springer, 2008, pp. 127-165.

[2] X. Bao and L. Chen, "Recent Progress in Distributed Fiber Optic Sensors," Sensors, vol. 12, pp. 8601-8639, 2012.

[3] A. Morana, S. Girard, E. Marin, C. Marcandella, P. Paillet, J. Périsse, J.-R. Macé, A. Boukenter, M. Cannas, and Y. Ouerdane , "Radiation tolerant fiber Bragg gratings for high temperature monitoring at MGy dose levels," Optics Letters, vol. 39, no. 18, pp. 5313-5316, 2014.

[4] X. Phéron, S. Girard, A. Boukenter, B. Brichard, S. D. Lesoille, J. Bertrand, and Y. Ouerdane, "High γ-ray dose radiation effects on the performances of Brillouin scattering based optical fiber sensors," *Opt. Express*, vol. 20, no. 24, pp. 26978-26985, 2012.

[5] C. Cangialosi, S. Girard, A. Boukenter, M. Cannas, S. Delepine-Lesoille, J. Bertrand, P. Paillet, Y. Ouerdane, "Hydrogen and radiation induced effects on performances of Raman fiber-based temperature sensors," *J. Lightwave Technol.*, vol. 33, no. 11, p. 1558-2213, 2015.

[6] C. Cangialosi, Y. Ouerdane, S. Girard, A. Boukenter, S. Delepine-Lesoille, J. Bertrand, C. Marcandella, P. Paillet, M. Cannas, "Development of a Temperature Distributed Monitoring System Based On Raman Scattering in Harsh Environment", IEEE Transactions on Nuclear Science, vol. 61 (6), 3315 – 3322, 2014.

[7] S. Rizzolo, A. Boukenter, E. Marin, M. Cannas, J. Perisse, S. Bauer, J-R. Mace, Y. Ouerdane, S. Girard, "Vulnerability of OFDR-based distributed sensors to high γ-ray doses," Opt. Express, vol. 23, no. 15, pp. 18997-19009, 2015.

[8] S. Rizzolo, E. Marin, M. Cannas, A. Boukenter, Y. Ouerdane, J. Perisse, S. Bauer, J-R. Mace, C. Marcandella, P. Paillet and S. Girard, "Radiation Effects on OFDR based sensors," *Optics Letters*, vol. 40, no. 20, pp. 4751-4754, 2015.

[9] B. J. Soller, D. K. Gifford, M. S. Wolfe and M. E. Froggatt, "High resolution optical frequency domain reflectometry for characterization of components and assemblies," *Opt. Express*, vol. 13, no. 2, pp. 666-674, 2005.

[10] S. Girard, J. Keurinck, Y. Ouerdane, J.-P. Meunier, and A. Boukenter, "Gamma-rays and pulsed X-ray radiation responses of germanosilicate single-mode optical fibers: influence of cladding codopants," *J. Lightwave Technol.*, vol. 22, no. 8, p. 1915–1922, 2004.

[11] E. J. Friebele, P. C. Schultz, and M. E. Gingerich, "Compositional effects on the radiation response of Ge-doped silica-core optical fiber waveguides," *Appl. Opt*, vol. 19, no. 17, p. 2910–2916, 1980.

[12] P. St. J. Russell, "Photonic-crystal fibers," *J. Lightwave Technol.*, vol. 24, no. 12, p. 4729–4749, 2006.

[13] S. Girard, J. Baggio, and J.-L. Leray, "Radiation-induced effects in a new class of optical waveguides: the airguiding photonic crystal fibers," *IEEE Trans. Nucl. Sci.*, vol. 52, no. 6, p. 2683–2688, 2005.

[14] G. Cheymol, H. Long, J. F. Villard, and B. Brichard, "High level gamma and neutron irradiation of silica optical fibers in CEA OSIRIS nuclear reactor," *IEEE Trans. Nucl. Sci.*, vol. 55, n° 14, p. 2252–2258, 2008.

[15] H. Henschel, J. Kuhnhenn, and U. Weinand, "High radiation hardness of a hollow core photonic bandgap fiber," in *8th European Conference on Radiation and Its Effects on Components and Systems, RADECS 2005*, 2005.

[16] L. Olanterä, C. Sigaud, J. Troska, F. Vasey, M. N. Petrovich, F. Poletti, N. V. Wheeler, J. P. Wooler, and D. J. Richardson, "Gamma irradiation of minimal latency Hollow-Core Photonic Bandgap Fibres," *Journal of Instrumentation*, vol. 8, 2013.

[17] S. Girard, A. Yahya, A. Boukenter, Y. Ouerdane, J.-P. Meunier, R. E. Kristiansen, and G. Vienne, "Gamma-radiation-induced attenuation in photonic crystal fibre," *IEE Electron. Lett.* , vol. 38, no. 20, p. 1169–1171, 2002.

[18] A. F. Kosolapov, I. V. Nikolin, A. L. Tomashuk, S. L. Semjonov, and M. O. Zabezhailov, "Optical losses in asprepared and gamma-irradiated microstructured silica-core optical fibers," *Inorg. Mater.*, vol. 40, no. 11, p. 1229–1232, 2004.

[19] S. Girard, Y. Ouerdane, M. Bouazaoui, C. Marcandella, A. Boukenter, L. Bigot, "Transient radiation-induced effects on solid core microstructured optical fibers," *Opt. Express*, vol. 19, no. 22, pp. 21760-21767, 2011.

[20] A. Chahadih, H. El Hamzaoui, O. Cristini, L. Bigot, R. Bernard, C. Kinowski, M. Bouazaoui and B. Capoen , "H2-induced copper and silver nanoparticle precipitation inside sol-gel silica optical fiber preforms," Nanoscale Research Letters , vol. 7, no. 1, p. 487 , 2012.

[21] I. Razdobreev, H. El Hamzaoui, G. Bouwmans, M. Bouazaoui, and V. B. Arion , "Photoluminescence of sol-gel silica fiber preform doped with Bismuth-containing heterotrinuclear complex," Optical Materials Express, vol. 2, no. 2, pp. 205-213, 2012.

[22] H. El Hamzaoui, L. Bigot, G. Bouwmans, I. Razdobreev, M. Bouazaoui, and B. Capoen , "From molecular precursors in solution to microstructured optical fiber: a Sol-gel polymeric route," *Opt. Mater. Express*, vol. 1, no. 2, pp. 234-242, 2011.

[23] S. Rizzolo, A. Boukenter, J. Périsse, G. Bouwmans, H. El Hamzaoui, L. Bigot, Y. Ouerdane, M. Cannas, M. Bouazaoui, J-R Macé, S. Bauer and S. Girard, "Radiation Response of OFDR Distributed Sensors Based on Microstructured Pure Silica Optical Fibers," in *15th European Conference on Radiation and Its Effects on Components and Systems (RADECS), 2015*, pp.1-3, 14-18 Sept. 2015.

[24] L. Skuja, "The origin of the intrinsic 1.9 eV luminescence band in glassy SiO_2," *J. Non-Cryst. Solids*, vol. 179, p. 51–69, 1994.

[25] L. Vaccaro, M. Cannas, S. Girard, A. Alessi, A. Morana, A. Boukenter, Y. Ouerdane, and R. Boscaino, "Influence of fluorine on the fiber resistance studied through the non-bridging oxygen hole center related luminescence", J. Applied Phys., vol.113, no.19, pp.193107,193107-5, 2013.